diameter; carbon dioxide is the only exception. Finally, the dual-mode sorption parameters, k_D and b, of all six gases in PPha-tere show a strong dependence on the condensability of the gas, similar to most other systems reported in the literature.

Acknowledgment. We are thankful to the donors of the Petroleum Research Fund, administered by the American Chemical Society, for partial support of this research. Financial assistance to N.F.B. provided by the National Consortium for Graduate Degrees for Minorities in Engineering is also highly appreciated.

References and Notes

(1) Kim, T. H.; Koros, W. J.; Husk, G. R.; O'Brien, K. C. *J. Membr. Sci.* **1988**, *37*, 45.
(2) Barbari, T. A.; Koros, W. J.; Paul, D. R. *J. Polym. Sci., Polym. Phys. Ed.* **1988**, *26*, 709.
(3) Masuda, T. H.; Tajima, H.; Yoshimura, T.; Higashimura, T. *Macromolecules* **1987**, *20*, 1467.
(4) Ichiraku, Y. S.; Stern, S. A.; Nakagawa, T. *J. Membr. Sci.* **1987**, *34*, 5.
(5) Sheu, F. R.; Chern, R. T. *J. Polym. Sci., Polym. Phys. Ed.* **1989**, *27*, 1121.
(6) Koros, W. J.; Chern, R. T. *Handbook of Separation Process Technology*; Rousseau, R. W., Ed.; John Wiley & Sons: New York, 1987; Chapter 20.
(7) Morgan, P. W. *Macromolecular Syntheses*; Wiley-Interscience: New York, 1978; p 413.
(8) Korshak, V. V. *J. Macromol. Sci., Rev. Macromol. Chem.* **1974**, *1*, 45.
(9) Huvard, G. S.; Stannett, V. T.; Koros, W. J.; Hopfenberg, H. B. *J. Membr. Sci.* **1980**, *6*, 185.
(10) Sanders, E. S.; Koros, W. J.; Hopfenberg, H. B.; Stannett, V. T. *J. Membr. Sci.* **1983**, *13*, 161.
(11) Sanders, E. S.; Koros, W. J.; Hopfenberg, H. B.; Stannett, V. T. *J. Membr. Sci.* **1984**, *18*, 53.
(12) Brown, N. F. MS Thesis, North Carolina State University, 1988.
(13) Chiou, J. S.; Paul, D. R. *J. Membr. Sci.* **1987**, *32*, 195.
(14) Koros, W. J.; Chan, A. H.; Paul, D. R. *J. Membr. Sci.* **1977**, *2*, 165.
(15) Erb, A. J.; Paul, D. R. *J. Membr. Sci.* **1981**, *8*, 11.
(16) Barbari, T. A.; Koros, W. J.; Paul, D. R. *J. Polym. Sci., Polym. Phys. Ed.* **1988**, *26*, 729.
(17) Paul, D. R. *Ber. Bunsen-Ges Phys. Chem.* **1979**, *83*, 294.
(18) Jolley, J. E.; Hilderbrand, J. H. *J. Am. Chem. Soc.* **1958**, *80*, 11050.
(19) Michaels, A. S.; Bixler, H. *J. Polym. Sci.* **1961**, *50*, 393.
(20) Shah, V. M.; Hardy, B. J.; Stern, S. J. *J. Polym. Sci., Polym. Phys. Ed.* **1986**, *24*, 2033.
(21) Koros, W. J.; Paul, D. R. *J. Polym. Sci., Polym. Phys. Ed.* **1981**, *19*, 1655.
(22) Fleming, G. K.; Koros, W. J. *Macromolecules* **1986**, *19*, 2285.
(23) Hilebrand, J. H.; Scott, R. L. *Solubility of Nonelectrolytes*, 3rd ed.; Reinhold: New York, 1950.
(24) Horuiti, H. *Pap. Inst. Phys. Chem. Rev.* **1931**, *117*, 125.
(25) Witchey, L. C.; Hopfenberg, H. B.; Chern, R. T., to be published in *J. Membr. Sci.*
(26) Witchey, L. C. Ph.D. Thesis, North Carolina State University, 1988.
(27) Paul, D. R.; Koros, W. J. *J. Polym. Sci., Polym. Phys. Ed.* **1976**, *14*, 675.
(28) Berens, A. R.; Hopfenberg, H. B. *J. Membr. Sci.* **1982**, *10*, 283.
(29) Reid, R. C.; Prausnitz, J. M.; Sherwood, T. K. *The Properties of Gases and Liquids*, 3rd ed.; McGraw-Hill: New York, 1977.
(30) Breck, D. W. *Zeolite Molecular Sieve*; Wiley-Interscience: New York, 1974; pp 634–640.
(31) Koros, W. J.; Paul, D. R.; Rocha, A. *J. Polym. Sci., Polym. Phys. Ed.* **1976**, *14*, 687.
(32) Toi, K.; Paul, D. R. *Macromolecules* **1982**, *15*, 1104.

Tridimensional Profile Functions in Structure Analysis of Crystalline Fibers by the "Whole-Pattern" Method. Dependence on Crystal Size and Crystallite Orientation

Pio Iannelli* and Attilio Immirzi

Dipartimento di Fisica, Università di Salerno, I-84100 Salerno, Italy.
Received June 15, 1989; Revised Manuscript Received September 20, 1989

ABSTRACT: With the aim of implementing crystal structure refinement programs applicable to fibrous materials and on the basis of the whole-pattern approach, theoretical functions have been developed expressing the continuous diffraction intensity versus crystal size and misalignment parameters. Applications of this function to two synthetic polymers, polyisobutylene and isotactic polypropylene, has afforded an excellent agreement between observed and calculated intensity.

Introduction

In recent papers[1,2] we have proposed a *whole-pattern* approach in structure refinement of crystalline fibrous materials, viz., a least-squares procedure using, as observations, the *continuous* diffracted intensities instead of the traditional *integrated* ones. To this end, we have studied bidimensional profile functions appropriate for describing the X-ray diffracted intensity recorded on photographic films, considering either cylindrical or flat-camera geometry. Starting from a modified Pearson-VII function, we have found, on empirical grounds, that the product of two Gauss functions is adequate to fit single reflections if a system of curvilinear film coordinates τ and ρ is chosen, which makes the shape of the recorded spots rectangular

$$\Phi(\tau_i, \rho_i) = f_\tau(\tau_i - \tau_k)\, f_\rho(\rho_i - \rho_k) \quad (1)$$

τ_i and ρ_i being the curvilinear coordinates of any point of the film and τ_k and ρ_k those of the *center* of the kth reflection.

In this paper a more exact approach is reported based on theoretical functions instead of empirical ones, also with the aim of obtaining, besides structural parameters refined, morphological parameters such as crystal sizes

0024-9297/90/2223-2375$02.50/0

and average angle of misalignment of oriented crystallites.

In the preceding papers we have considered the intensity distribution on the film (two dimensions). In the present case we shall consider the reciprocal space (three dimensions), both to render the fit independent of the diffraction geometry and to account for possible dimensional asymmetry of crystallites. Although several theoretical expressions, either applicable in film space or in the reciprocal space, have been already published,[3-5] we have opted for profile functions of more practical use and as simple as possible in view of using them in structure-refinement least-squares fitting programs with nonprohibitive computer time consumption.

Crystalline fibers of polyisobutylene (PIB) and isotactic polypropylene (IPP) have been considered as testing materials for verifying the feasibility of the profile functions obtained.

Experimental Section

The PIB used in this paper was the high molecular weight commercial product by EGA–Chemie (catalog no. 18 149-8, MW ~200 000), the same as studied in refs 2 and 6. Crystalline and oriented samples were obtained by simple elastic stretching of a piece of material. The IPP sample used in this paper, the same as studied in refs 1 and 7, was obtained stretching at 140 °C and annealing at 140 °C for 3 h.

The X-ray fiber diffraction patterns (Ni-filtered Cu Kα radiation) were recorded by using a cylindrical camera operating under vacuum (nominal radius 57.30 mm) taking four distinct spectra with exposures in the ratios 1, 1.5, 9, and 12 for PIB sample and three in the ratios 1, 1.3, and 3.6 for IPP sample. Each film (Eastman Kodak DEF-5) was digitized by a photoscan instrument (Optronics System P-1000, Model 30D) according to a 100 × 100 μm grid. The digitized pattern was centered to obtain the x and y axes exactly coincident with the meridional and equatorial directions of the fibers. The preliminary data processing for obtaining diffraction intensity data from the optical density measurements followed the procedure outlined in refs 1 and 2. Like in the preceding papers, the background intensity due to incoherent scattering and to the amorphous material was not subtracted ab initio and was considered at the subsequent least-squares fitting stage.

Intensity Function

A crystal of infinite size diffracts only in discrete directions, corresponding to discrete points in reciprocal space (Bragg points), with intensities proportional to F_k^2, F_k being the structure factor for each reflection (k stands for the hkl Bragg indices). If the crystal is, instead, of finite size, diffraction takes place in extended regions surrounding the Bragg points. When the reciprocal space notation is introduced and fractional reciprocal coordinates ξ, η, and ζ (ξ, η, and ζ are zero on the Bragg points) are used, the diffracted intensity is proportional to the product $F_k^2\, L(\xi,\eta,\zeta)$, $L(\xi,\eta,\zeta)$ being the Laue function

$$L(\xi,\eta,\zeta) = L(\xi)\, L(\eta)\, L(\zeta) = \frac{\sin^2(\pi N_a aa^*\xi)}{\sin^2(aa^*\xi)} \frac{\sin^2(\pi N_b bb^*\eta)}{\sin^2(bb^*\eta)} \frac{\sin^2(\pi N_c cc^*\zeta)}{\sin^2(cc^*\zeta)} \quad (2)$$

where N_a, N_b, and N_c are the number of unit cells along the directions of a, b, and c edges and a^*, b^*, and c^* are the corresponding reciprocal lattice constants. The Laue function, which reduces to a δ-function when the crystal becomes infinite, is well approximated by the function ($N_t = N_a N_b N_c$)[8]

$$L(\xi,\eta,\zeta) = N_t^2 \exp\{-\pi[(N_a aa^*\xi)^2 + (N_b bb^*\eta)^2 + (N_c cc^*\zeta)^2]\} \quad (3)$$

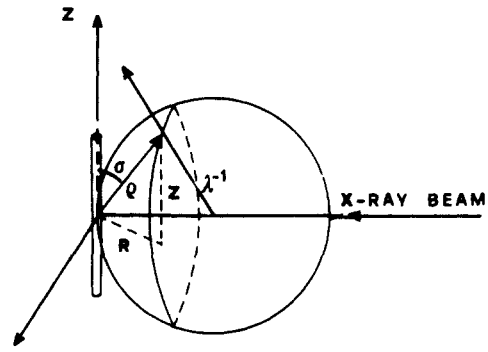

Figure 1. Polar coordinates in reciprocal space.

As the Gaussian function $\exp(-x^2)$ is fast decreasing, the diffracted intensity is practically significant only within a limited space surrounding the Bragg point whose boundary surface is a sphere in the orthorhombic cases with $N_a = N_b = N_c$ and an ellipsoid in other cases. In any case the size and the shape of the figures are independent on hkl indices.

In the case of fibrous samples, containing particles cylindrically distributed around the fiber axis and preferentially oriented parallel to it, the three-dimensional intensity function must be averaged affording a two-dimensional intensity function, which can be conveniently referred to the variables ρ and σ defined in Figure 1. In this case Holmes and Barrington Leigh[9] obtained the following expression for the *intensity function*, I_s

$$I_s(\rho,\sigma) = \frac{1}{\alpha_0}\int I_p \exp\left[\left(-\frac{(\sigma_p - \sigma_s)^2}{2\alpha_0^2}\right)\right] i_0 \times \left[\frac{\sin\sigma_p \sin\sigma_s}{\alpha_0^2}\right] \sin\sigma_p\, d\sigma_p \quad (4)$$

where index p stands for *particle* (not necessarily crystal) and s for *sample*; ρ is the reciprocal scattering vector solid with the particle (ρ_p) or the sample (ρ_s); σ_p and σ_s are the angles between ρ_p and ρ_s with the preferred orientation (see Figure 1); i_0 is the Bessel function of the second kind of order zero; I_p is proportional to the square of the scattering factor of the single particle. The above relationship is valid under the hypothesis that the distribution of the particles with respect to the preferred orientation is given by

$$\mathcal{N}(\alpha) = \frac{1}{2\pi\alpha_0^2}\exp\left(-\frac{\alpha^2}{2\alpha_0^2}\right) \quad (5)$$

where α is the angle between the axis of a single particle and the preferred orientation axis and α_0 is a misalignment parameter. On this basis, Fraser et al.[10] obtained a complex expression for the intensity function in the case of a fibrous material made of crystalline particles having an orthorhombic unit cell. They replaced I_p with the convolution about the fiber axis of the intensity function of the single crystallite.

To obtain expressions applicable to the triclinic case and to get expressions more handy for computation, we have preferred a different route expressing the intensity function as the convolution of the alignment distribution function about the fiber axis with the convolute Laue function, i.e., the cylindrically averaged Laue function, by rotation about the fiber axis. The former is representable in a simple way by the normalized Gaussian distribution (crystallite distribution function, cdf)

$$\mathcal{N}(\alpha) = \frac{2(\ln 2)^{1/2}}{\pi^{1/2}\alpha_0}\exp\left[-4\ln 2\left(\frac{\alpha}{\alpha_0}\right)^2\right] \quad (6)$$

where α_0 is the half-height peak width of the distribution. The latter is given, for each hkl reflection (shortly k), by the integral

$$\mathcal{L}_k(\Delta R_k,z) = \frac{1}{2\pi R}\int_0^{2\pi R} L(\xi)\, L(\eta)\, L(\zeta)\, ds \qquad (7)$$

which is taken along the whole circle of radius R (equatorial component of the reciprocal scattering vector), in practice along a short arc where the Laue function is appreciably nonzero. ΔR_k is the difference between R and R_k (R value at the Bragg point) and z is taken, as below, parallel to fiber axis. $\mathcal{L}_t(\Delta R_k,z)$ is a toroidal function whose shape depends not only on R but also on the k indices. Moreover, crystallographically symmetrical reflections, such as hkl and $\bar{k}hl$ in tetragonal cases, might have different $\mathcal{L}$ functions if $N_a \neq N_b$.

To evaluate the integral in eq 7, it is practical to introduce (see Figure 2A) a Cartesian frame with the origin at the center of the hkl reflection, the x axis coincident with the R_k vector, and the z axis parallel to the fiber axis. If the Laue function is nonzero only in a small region, and excepting meridional reflections, the integral along the circular arc crossing the Bragg position reduces to a linear integral along y. Fractional reciprocal coordinates ξ, η, and ζ are related to x, y, and z (Å^{-1} units) through the matrix multiplication

$$\{\xi,\eta,\zeta\} = \mathbf{C}\cdot\mathbf{M}\cdot\{x,y,z\} \qquad (8)$$

where the 3×3 diagonal matrix $\mathbf{C}$ has the diagonal terms $1/a^*$, $1/b^*$, and $1/c^*$, $\mathbf{M} = (\mathbf{B} \times \mathbf{A})^{-1}$, and $\mathbf{A}$ and $\mathbf{B}$ are, respectively (ω is the angle between ξ and x axes; see Figure 2):

$$\mathbf{A} = \begin{pmatrix} 1 & \cos\gamma^* & \cos\beta^* \\ 0 & \sin\gamma^* & -\cos\alpha\sin\beta^* \\ 0 & 0 & 1/cc^* \end{pmatrix} \qquad (9)$$

$$\mathbf{B} = \begin{pmatrix} \cos\omega & \sin\omega & 0 \\ -\sin\omega & \cos\omega & 0 \\ 0 & 0 & 1 \end{pmatrix} \qquad (10)$$

Introducing also the 3×3 diagonal matrix $\mathbf{D}$ whose diagonal terms are $\pi(N_a/a^*)^2 = \pi(\Delta a/aa^*)^2$, $\pi(N_b/b^*)^2 = \pi(\Delta b/bb^*)^2$, and $\pi(N_c/c^*)^2 = \pi(\Delta c/cc^*)^2$, with Δa, Δb, and Δc the crystallites dimensions in angstroms along a, b, and c edges, one obtains for eq 3

$$L(x,y,z) = N_t^2 \exp[-(x,y,z)\cdot\mathbf{U}\cdot\{x,y,z\}] \qquad (11)$$

where

$$\mathbf{U} = \tilde{\mathbf{M}}\cdot\mathbf{D}\cdot\mathbf{M} \qquad (12)$$

By means of eq 11 and recalling that $\Delta R_k = x$, the integral in eq 7 becomes

$$\mathcal{L}_k(\Delta R_k,z) = \frac{N_t^2}{2\pi R}\int_{-\infty}^{\infty}\exp[-(\Delta R_k,y,z)\cdot\mathbf{U}\cdot\{\Delta R_k,y,z\}]\, dy \qquad (13)$$

Using the known integral[11]

$$\int \exp -(ax^2 + 2bx + c)\, dx = \frac{1}{2}\left(\frac{\pi}{a}\right)^{1/2}\exp\frac{b^2-ac}{a}\,\mathrm{erf}\left(a^{1/2}x + \frac{b}{a^{1/2}}\right) + \text{constant} \qquad (14)$$

one obtains finally

$$\mathcal{L}_k(\Delta R_k,z) = \frac{N_t^2}{2\pi R}\left(\frac{\pi}{U_{22}}\right)^{1/2}\exp[-(\Delta R_k,z)\cdot\mathbf{L}\cdot\{\Delta R_k,z\}] \qquad (15)$$

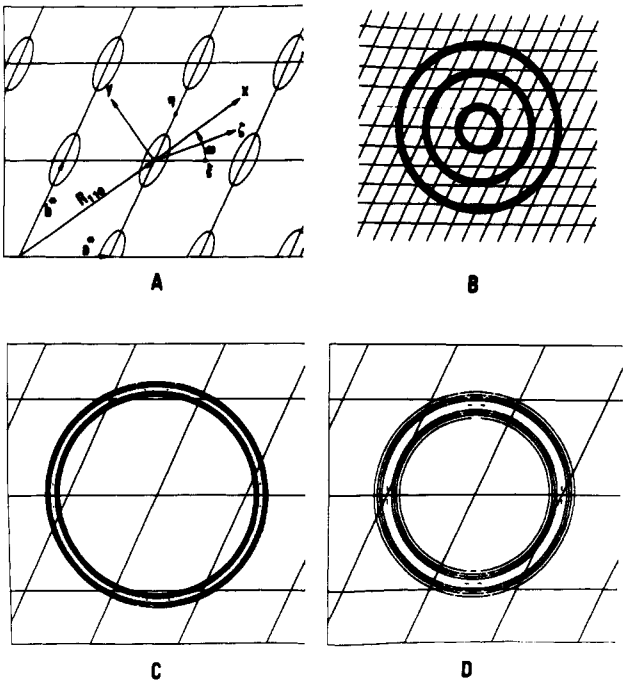

Figure 2. Representation of the Laue function on the a^*b^* plane and some of its convolutions with different hkl indices for a hypothetical triclinic cell with a = 10.0 Å, b = 8.0 Å, c = 12.0 Å, α = 102°, β = 114°, and γ = 107°. (A) The Cartesian frame x,y,z applicable to the (110) reflection is also shown (z is perpendicular to the plane). (B) T_{010}, T_{300}, T_{320}, (C) T_{010}, and (D) T_{100} torus projections on the a^*b^* plane for the same cell parameters of Figure 2A and with crystal dimensions Δa = 50 Å, Δb = 150 Å, Δc = 50 Å, and α_0 = 0°.

where $\mathbf{L}$ is the 2×2 matrix

$$\mathbf{L} = \frac{U}{U_{22}}\begin{pmatrix} U^{33} & -U^{13} \\ -U^{31} & U^{11} \end{pmatrix} \qquad (16)$$

and U is the determinant of the $\mathbf{U}$ matrix.

As discussed above, $\mathcal{L}_k(\Delta R_k,z)$ in eq 15, termed later the *cylindrical crystallite profile function* (ccpf), has cylindrical symmetry in the reciprocal space and toroidal shape and depends on the hkl indices.

At this point the intensity function T_k for the whole sample can be obtained as the convolution $\mathcal{N}(\alpha)\ \mathcal{L}_k(\Delta R_k,z)$ of the cdf and the ccpf. To evaluate the convolution, it is useful to introduce a new reference frame $x'y'z'$ by rotating xyz about y by the angle $(\pi/2) - \sigma_k$, so rendering x' coincident with ρ (Figure 3). Thus, the crystallite misalignment α occurs in the plane $x'z'$ and, since α is small, the integration along the circular path $\rho\alpha$ is equivalent to a linear integration along z'. As the vector $(\Delta R,z)$ is related to the $(\Delta\rho_k,\rho\alpha)$ vector ($\Delta\rho_k = \rho - \rho_k$) through the operation

$$\{\Delta R_k,z\} = \mathbf{S}\cdot\{\Delta\rho_k,\rho\alpha\} \qquad (17)$$

with

$$\mathbf{S} = \begin{pmatrix} \sin\sigma_k & -\cos\sigma_k \\ \cos\sigma_k & \sin\sigma_k \end{pmatrix} \qquad (18)$$

eq 15 becomes

$$\mathcal{L}_k(\Delta\rho_k,\rho\alpha) = \frac{N_t^2}{2\pi R}\left(\frac{\pi}{U_{22}}\right)^{1/2}\exp[-(\Delta\rho_k,\rho\alpha)\cdot\mathbf{Q}\cdot\{\Delta\rho_k,\rho\alpha\}] \qquad (19)$$

with $\mathbf{Q} = \tilde{\mathbf{S}}\cdot\mathbf{L}\cdot\mathbf{S}$. Considering that $\alpha = \sigma - \sigma_k = \Delta\sigma_k$, the convolution between cdf and ccpf is given by

$$T_k(\Delta\rho_k,\Delta\sigma_k) = \int_{-\infty}^{+\infty}\mathcal{L}_k(\Delta\rho_k,\Delta\sigma_k - u)\cdot\mathcal{N}(u)\, du \qquad (20)$$

where the integration interval can be choosen from $-\infty$ to $+\infty$ inasmuch $\mathcal{N}(u)$ is fast decreasing with $|u|$.

Using again eq 14, one obtains

$$T_k(\Delta\rho_k,\Delta\sigma_k) = \frac{N_t^2(\ln 2)^{1/2}}{\pi^{1/2}\alpha_0 R}\left[U_{22}\left(\frac{4\ln 2}{\alpha_0^2} + P_{22}\rho^2\right)\right]^{-1/2} \times \exp[-P\rho^2\Delta\rho_k^2]\exp\left[-\frac{4\ln 2}{\alpha_0^2}(\Delta\rho_k,\rho\Delta\sigma_k)\cdot\mathbf{P}\cdot\{\Delta\rho_k,\rho\Delta\sigma_k\}\right] \quad (21)$$

where $\mathbf{P} = \mathbf{S}\cdot\mathbf{L}\cdot\tilde{\mathbf{S}}$ and P is the determinant of $\mathbf{P}$.

Intensity Function and Diffraction Pattern Fitting

Equation 21 allows calculating, for fibrous samples of polymeric crystalline materials, the continuous diffracted intensity for any reflection in the neighborhood of Bragg position:

$$I_k(\rho_i,\sigma_i) = F_k^2\, T_k(\rho_i-\rho_k,\sigma_i-\sigma_k) \quad (22)$$

As several more or less overlapped reflections may contribute to a given point, the total diffracted intensity at point ρ_i,σ_i is given by

$$I(\rho_i,\sigma_i) = \sum_k F_k^2\, T_k(\rho_i-\rho_k,\sigma_i-\sigma_k) + B(\rho_i,\sigma_i) \quad (23)$$

where the sum is extended over all reflections whose Bragg points ρ_k,σ_k are close to the current ρ_i,σ_i point. $B(\rho_i,\sigma_i)$ is the diffused diffraction intensity due to amorphous material and air (see below). Note that eq 21 is independent of the type of camera used. In each case measurements made on a photographic film can always be referred to the appropriate ρ_i,σ_i coordinates.

The $B(\rho_i,\sigma_i)$ diffused intensity has been parametrized considering that, in the polymer case, there might be, in general, (i) an isotropic contribution of uncoherent scattering, decreasing with increasing ρ_i and dependent on σ_i; (ii) a contribution of amorphous and unoriented material appearing on the spectrum as one or several haloes, which depend only on ρ_i; (iii) a contribution of diffraction of noncrystalline but oriented material appearing in the spectra as one or several streaks orthogonal to the fiber axis. Thus $B(\rho_i,\sigma_i)$ has been parametrized as the sum of three contributions in the following form:

$$B(\rho_i,\sigma_i) = B^{(u)}(\rho_i) + B^{(i)}(\rho_i) + B^{(a)}(\rho_i,\sigma_i) \quad (24.1)$$

$$B^{(u)}(\rho_i) = \epsilon_1 + \epsilon_2\rho_i + \epsilon_3\rho_i^2 \quad (24.2)$$

$$B^{(i)}(\rho_i) = \sum_m \frac{g_m^{(1)}}{g_m^{(2)}}\exp\left[-\left(\frac{\rho_i - g_m^{(3)}}{g_m^{(2)}}\right)^2\right] \quad (24.3)$$

$$B^{(a)}(\rho_i,\sigma_i) = \sum_m \frac{f_m^{(1)}}{f_m^{(2)}f_m^{(3)}}\exp\left[-\left(\frac{\rho_i\sin(\sigma_i) - f_m^{(4)}}{f_m^{(2)}}\right)^2\right] \times \exp\left[-\left(\frac{\rho_i\cos(\sigma_i) - f_m^{(5)}}{f_m^{(3)}}\right)^2\right] \quad (24.4)$$

In the PIB case the fiber diffraction pattern displays only isotropic diffused intensity with a single halo, so only $B^{(u)}(\rho_i)$ and $B_1^{(i)}(\rho_i)$ terms have been considered with 3 + 3 parameters altogether. In the IPP case an equatorial diffused streak is present and so $B^{(u)}(\rho_i)$ and $B_1^{(a)}(\rho_i,\sigma_i)$ have been considered with 3 + 4 parameters altogether ($f_1^{(5)} = 0$).

Having established theoretical relationships for calculating the diffracted intensity as a function of structural parameters (affecting F_k) and morphological parameters (affecting T_k), a fitting procedure can be implemented for adjusting both structural and morphological parameters starting from coarse values. This may be done, for instance, by means of the least-squares method, minimizing the quantity

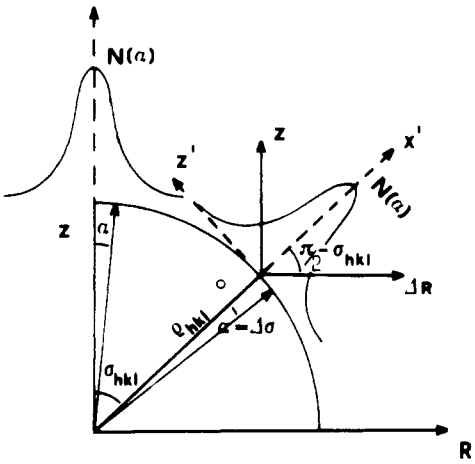

Figure 3. Effect of the cdf on the broadening of a reciprocal space point. The Cartesian frame used to obtain eq 18 is also shown.

$$\sum_i w_i[I_{obsd}(\rho_i,\sigma_i) - S\,I(\rho_i,\sigma_i)]^2 \quad (25)$$

where w_i are the statistical weight of the observations $I_{obsd}(\rho_i,\sigma_i)$ and S is a scale factor.

Our purpose is to carry out this fitting procedure in the cases of polyisobutylene (PIB) and isotactic polypropylene (IPP) and to compare the results with those obtained using empirical profile functions.[1,2] Before undertaking a structural refinement process, however, we have carried out a fit adjusting only the morphological parameters and the parameters controlling $B(\rho_i,\sigma_i)$ (see above), treating F_k^2 values as independently adjustable quantities. The observational equation for this process, considering that I_{obsd} values are measured on several films, is

$$I(\rho_i,\sigma_i) = S_j[\sum_k F_k^2\, T_k(\rho_i-\rho_k,\sigma_i-\sigma_k) + B(\rho_i,\sigma_i)] \quad (26)$$

where as many scale factors S_j are considered as is the number of films measured. S_j values are initially set to values proportional to the exposures and subsequently adjusted together with the other parameters.

The preliminary fit, based on observational equations (eq 26), was performed by means of a least-squares procedure, which utilizes the Gauss–Newton approach, i.e., the linearization of the observational equations and determination of corrected values by an iterative process. The regression was done using the regions of the diffraction pattern shown in Figure 4 which are inclusive from the 0th to the 5th layer (PIB) and from the 0th to the 2nd layer (IPP). The optimized quantities were (i) the crystallite dimensions Δa, Δb, and Δc, (ii) the misalignment parameter, α_0, (iii) the diffused diffraction parameters, the scale factors, and the camera radius, (iv) the squared structure factors F_k^2, and (v) the lattice constants (in IPP case only). When exact (or almost exact) overlap occurs among reflections, F_k^2 have been adjusted by keeping their ratios constants (the ratios were set equal to the corresponding F_{calcd}^2 values obtained in previous analyses.[1,2]

The optimization of the parameters above was performed by iterating the least-squares procedure until very low shift to standard error ratios were obtained. The

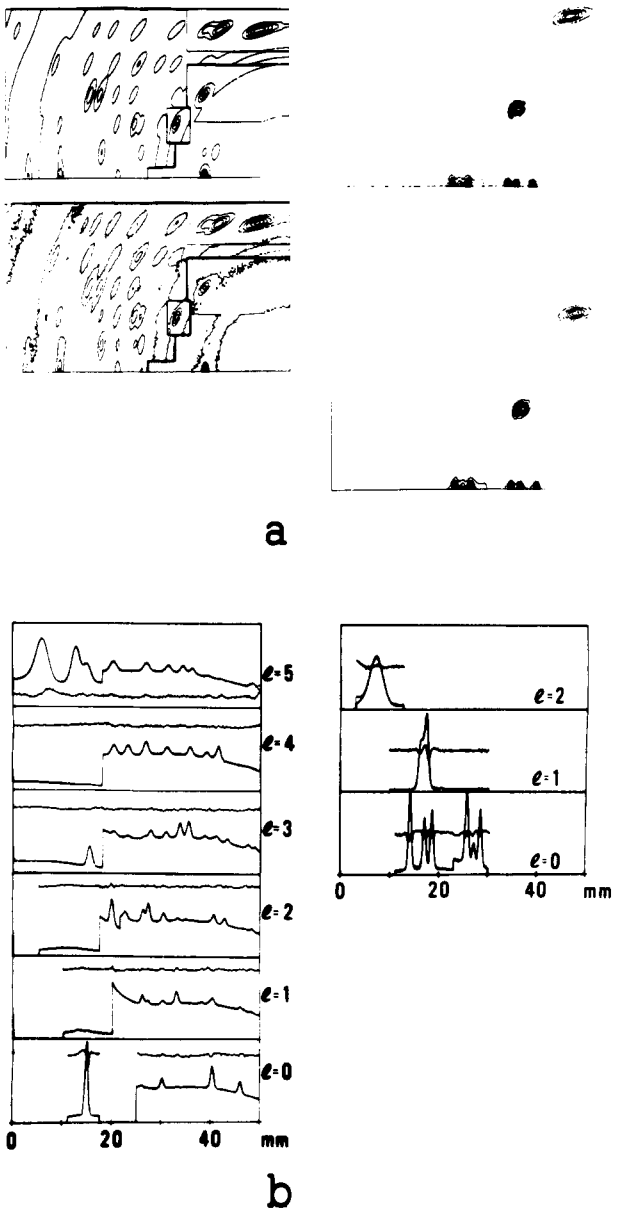

Figure 4. Comparison between observed and calculated spectra for PIB (left) and IPP (right). In a the whole calculated (up) and observed (down) bidimensional spectra are represented by level lines. In b the observed (thin line) and calculated (thick line) spectra, practically coincident, are compared only along the layers line. The difference (continuous thick line) between observed and calculated intensities are also shown.

weight factors, w_i, have been assumed to be unitary. The agreement index, $R = \sum|I_{obsd} - I_{calcd}|/\sum I_{obsd}$, has been evaluated cycle by cycle. The reflections included in the calculation are those contributing to the film regions considered and having $F_{calcd} > 1.3$ electrons/cell. They are 96 in the PIB case and 19 in the IPP case. The final results, with the exceptions of the F_k^2 values, are reported in Table I together with the standard errors. By means of the Δa, Δb, and Δc refined values in Table I, we have evaluated the crystallite size in the direction normal to the (110), (130), and (040) planes. The values obtained, respectively, 159, 121, and 115 Å, are comparable with those found by Morosoff et al.[12] (157, 120, and 134 Å) in the case of IPP fiber annealed for 1000 min at 140 °C.

Figure 4 shows the comparison between the observed and calculated spectra, either considering one-dimensional sections along the layer lines or considering the whole bidimensional spectrum represented by level lines.

Table I
Structural and Nonstructural Parameters Resulting at the End of the Refinement Performed[a]

	PIB	IPP
Δa, Å	127.3 (9)	121.2 (4)
Δb, Å	107.8 (8)	115.2 (3)
Δc, Å	73.2 (2)	80.3 (1)
α_0, deg	5.60 (1)	3.780 (6)
a, Å	6.88	6.66 (1)
b, Å	11.91	20.78 (1)
c, Å	18.60	6.50 (1)
cos α	0.0	0.0
cos β	0.0	−0.1479 (1)
cos γ	0.0	0.0
S_1	0.0792 (3)	1.65 (1)
S_2	0.1265 (4)	2.10 (2)
S_3	0.632 (1)	6.04 (3)
S_4	0.913 (2)	
ϵ_1	−110.8 (9)	3.83 (7)
ϵ_2	1112 (5)	−11.9 (5)
ϵ_3	−1433 (6)	11.5 (9)
g_1	19.0 (2)	
g_2	0.0842 (2)	
g_3	0.1477 (3)	
f_1		0.0056 (1)
f_2		0.093 (1)
f_3		0.0136 (1)
f_4		0.206 (1)
f_5		0.0
camera radius, mm	57.56 (1)	57.21 (2)
no. of points	150000	105350
R_1	0.077	0.057
R_2	0.088	0075
R_3	0.037	0.063
R_4	0.020	

[a] Δa, Δb, and Δc are the crystal sizes appearing in the matrix **D** (see eq 12 and preceding paragraph); α_0 is the average angle of misalignment of oriented crystallites (see eq 6); a, b, c, α, β, and γ are the lattice constants; S_i values (see eq 26) are the scale factors converting absolute intensities (electrons/cell)^2 into arbitrary units; ϵ_i, g_i, and f_i are the parameters expressing the diffused diffraction intensity of noncrystalline material (see eq 24.1–4); R_j values are the R indices $\sum|I_{obsd,i} - I_{calcd,i}|/\sum I_{obsd,i}$ evaluated for the four (PIB case) and three (IPP case) films separately. The standard errors indicated in parentheses are those resulting from the diagonal terms of the inverted normal matrix and are, possibly, underestimated.

Conclusion

The visual comparison between observed and calculated fiber spectra and the low value of disagreement indices obtained in the nonstructural full-pattern refinement indicate that the profile functions are adequate to analytically reproduce fiber spectra of polymers. It is particularly significant that only four morphological parameters are sufficient to reproduce the peak widths, both along 2θ-constant and 2θ-variable directions, *within the whole spectrum.*

Although the diffraction of the noncrystalline function has been treated with rather arbitrary functional forms, the values of nonmorphological parameters obtained should be scarcely influenced by this arbitrariness because of the broadness of this contribution.

An application of the full-pattern crystal structure refinement based on the profile functions discussed in this paper is now in progress.

Acknowledgment. The financial support by Ministero della Pubblica Istruzione and by Consiglio Nazionale delle Ricerche (Strategic Project on Advanced Crystallographic Methods) is acknowledged.

References and Notes

(1) Immirzi, A.; Iannelli, P. *Macromolecules* **1988**, *21*, 768.

(2) Iannelli, P.; Immirzi, A. *Macromolecules* **1989**, *22*, 200.
(3) Makowski, L. *Fiber Diffraction Methods*; French & Gardner, Ed.; ACS Symposium Series 141; American Chemical Society: Washington, DC, 1980; Chapter 8, p 139.
(4) Fraser, R. D. B.; MacRae, T. P.; Miller, A.; Rowlands, R. J. *J. Appl. Cryst.* **1976**, *9*, 81.
(5) Millane, R.; Arnott, S. *J. Macromol. Sci., Phys.* **1985-1986**, *B24* (1-4), 193.
(6) Iannelli, P.; Immirzi, A. *Macromolecules* **1989**, *22*, 196.
(7) Immirzi, A.; Iannelli, P. *Gazz. Chim. Ital.* **1987**, *117*, 201.
(8) Vainshtein, *Diffraction of X-ray by Chain Molecules*; Elsevier Publishing Company: Amsterdam, The Netherlands, 1966; p 344.
(9) Holmes, K. C.; Barrington Leigh, J. *Acta Crystallogr.* **1974**, *A30*, 635.
(10) Fraser, R. D. B.; Suzuki, E.; MacRae, T. P. *Structure of Crystalline Polymers*; Elsevier Applied Science Publishers: Hall, I., Ed.; Chapter 1, p 1.
(11) Abramowitz, Stegun, *Handbook of Mathematical Functions*, Dover Publications, Inc.: New York, 1970; p 303.
(12) Morosoff, N.; Sakaoku, K.; Peterlin, K. *J. Polym. Sci., Part A-2* **1972**, *10*, 1221.

Time-Resolved Small-Angle X-ray Scattering of a High Density Polyethylene/Low Density Polyethylene Blend

H. H. Song,[†] D. Q. Wu,[†] B. Chu,[*,†] M. Satkowski,[‡] M. Ree,[‡] R. S. Stein,[‡] and J. C. Phillips[§]

Department of Chemistry, State University of New York at Stony Brook, Long Island, New York 11794-3400, Polymer Research Institute, University of Massachusetts, Amherst, Massachusetts 01003, and SUNY Beamline X3, NSLS, Brookhaven National Laboratories, Upton, New York 11970. *Received May 11, 1989; Revised Manuscript Received August 1, 1989*

ABSTRACT: The semicrystalline morphology of a 50/50 blend of high density polyethylene/low density polyethylene (HDPE/LDPE) was studied by time-resolved small-angle X-ray scattering (SAXS) using the State University of New York (SUNY) Beamline at the National Synchrotron Light Source (NSLS). The HDPE/LDPE blend, which was cooled slowly at a cooling rate of 0.3 °C/min, showed an interfibrillar scale separation within the spherulites that contained both the HDPE and the LDPE component. On the other hand, the same polymer blend, which was cooled rapidly at a cooling rate of 110 °C/min, appeared to show separation of HDPE and LDPE on an interlamellar scale. When the blend was quickly cooled to two successive temperatures, the scattering profiles were similar in nature to those obtained from the same sample that was directly quenched. The two-step rapid cooling represented quenching (1) from ~125 °C, which was above the HDPE crystallization temperature, to 110 °C, which was lower than the HDPE crystallization temperature but higher than the LDPE crystallization temperature, and (2) from 110 to 100 °C, which was below the LDPE crystallization temperature, while the direct rapid cooling was from 135 to 65 °C.

Introduction

Fractionation is known to occur when a polydisperse polymer undergoes crystallization.[1-4] Such a phenomenon is also seen in quasi-binary polymer pairs.[5-9] Of particular interest is the structural arrangement of the two components in a binary blend. Small-angle X-ray scattering (SAXS) can be used to measure the lamellar structure in crystalline polymers. The advent of a higher intensity synchrotron X-ray source[9-11] has made the SAXS technique even more powerful since the crystallization behavior can be studied in the time-resolved mode.

Shultz[12] studied the crystallization of linear polyethylene (LPE) by SAXS. At low crystallization temperatures, the long periods formed by LPE were independent of time. At higher crystallization temperatures, the long periods decreased with time, indicating the formation of new crystallites between the earlier formed lamellae. Rault[13] et al. studied a 50/50 blend of high density polyethylene (HDPE) and low density polyethylene (LDPE) by static SAXS. They described the scattering in terms of a paracrystalline model having a bimodal distribution of crystalline widths.

In our previous study[9] with synchrotron radiation, the lamellar structure of a 50/50 blend of HDPE and LDPE was observed during crystallization under fast cooling (110 °C/min). The results showed that for all three samples (HDPE, LDPE, and 50/50 blend) the lamellar spacing decreased during crystallization and was accompanied by the appearance of a marked hump in the SAXS patterns. The results were interpreted in terms of the ordering of the lamellar structure and the growth of new crystallites in the amorphous zones between the lamellae. In the 50/50 blend, the SAXS results suggested that HDPE and LDPE crystallized separately on an interlamellar scale. In this study we extend our previous SAXS work to two different crystallization conditions. In the first case, the blend was crystallized at a slow cooling rate (0.3 °C/min). Under the second condition, the blend was isothermally crystallized at two different temperatures, T_H and T_L in succession (110 °C/min) where T_H denotes a temperature lower than the crystallization temperature of HDPE but still high enough to keep LDPE in the melt

* Author to whom all correspondence should be addressed.
† State University of New York at Stony Brook.
‡ University of Massachusetts.
§ Brookhaven National Laboratories.

0024-9297/90/2223-2380$02.50/0